nature nanotechnology

ARTICLES

PUBLISHED ONLINE: 7 SEPTEMBER 2014 | DOI: 10.1038/NNANO.2014.183

Generation and electric control of spin–valley-coupled circular photogalvanic current in WSe_2

Hongtao Yuan[1,2], Xinqiang Wang[3,4], Biao Lian[1], Haijun Zhang[1], Xianfa Fang[3,4], Bo Shen[3,4], Gang Xu[1], Yong Xu[1], Shou-Cheng Zhang[1,2], Harold Y. Hwang[1,2]* and Yi Cui[1,2]*

The valley degree of freedom in layered transition-metal dichalcogenides provides an opportunity to extend the functionalities of spintronics and valleytronics devices. The achievement of spin-coupled valley polarization induced by the non-equilibrium charge-carrier imbalance between two degenerate and inequivalent valleys has been demonstrated theoretically and by optical experiments. However, the generation of a valley and spin current with the valley polarization in transition-metal dichalcogenides remains elusive. Here we demonstrate a spin-coupled valley photocurrent, within an electric-double-layer transistor based on WSe_2, whose direction and magnitude depend on the degree of circular polarization of the incident radiation and can be further modulated with an external electric field. This room-temperature generation and electric control of a valley and spin photocurrent provides a new property of electrons in transition-metal dichalcogenide systems, and thereby enables additional degrees of control for quantum-confined spintronic devices.

Generation and manipulation of a spin current is one of the most critical steps in developing semiconductor spintronics applications[1–3]. In a two-dimensional electronic system (2DES) with spin degeneracy lifted, irradiation with circularly polarized light can result in a non-uniform distribution of photo-excited carriers in k-space following optical selection rules and energy/momentum conservation, which finally leads to a spin current[4–6]. Referred to as the circular photogalvanic effect (CPGE)[7–10], the fingerprint of such a spin photocurrent is the dependence on the helicity of the light. As schematically shown in Fig. 1a, in a Rashba 2DES[11,12], the absorption of circularly polarized light results in optical spin orientation by transferring the angular momentum of photons to electrons, and thus, the non-equilibrium spin polarization of electrons forms a spin current with electron motion in the 2DES plane. Generally, the amplitude of the CPGE current can be expressed by $j_{CPGE} = \eta\gamma I \sin\theta \sin 2\varphi$ (ref. 7) where η is the absorbance, γ is the matrix element related to the spin, orbital and symmetry of the 2DES, I is the incident light intensity, θ is the incident angle (Fig. 1b) and φ is the rotation angle of the quarter-wave plate (reflecting the helicity of the incident circularly polarized radiation). This electric current has two important characteristic features: (1) its direction and magnitude depend on the degree of circular polarization of the incident light, as indicated in Fig. 1b, and (2) it can be controlled via modulating the γ coefficient, which is of practical significance for spin–current control.

In transition-metal dichalcogenides MX_2 (M = Mo, W; X = S, Se, Te), which have a layered honeycomb lattice and two inequivalent valleys in the k-space electronic structure in the hexagonal Brillouin zone, as a result of the large separation of valleys in k-space and the resulting suppression of intervalley scattering, the valley index can be used in analogy to the spin in spintronics, opening a new research direction called 'valleytronics'[13–15]. Such valley polarization achieved via valley-selective circular dichroism has been demonstrated theoretically and experimentally in those MX_2 systems that do not have inversion symmetry (in monolayer cases or under an electric field)[13,14,16–22]. However, a spin–valley current in MX_2 compounds caused by such a valley polarization has not been observed, and neither has its electric-field control. In this Article, we present, using a circularly polarized optical excitation on WSe_2 electric-double-layer transistors (EDLTs), the first observation of a spin-coupled valley photocurrent whose direction and magnitude depend on the degree of circular polarization of the incident light and can be controlled continuously by the external electric field. It was theoretically found that, owing to the modulation of the degree of broken inversion symmetry, the two valleys can possess different optical selection rules for the generation of a spin-coupled valley photocurrent.

Inversion symmetry breaking in WSe_2 induced by surface band bending. Similar to other layered MX_2 crystals, 2H-WSe_2 is composed of two formula units by stacking the Se–W–Se sandwiched structure (a monolayer unit with D_{3h} symmetry) nonsymorphically along the c axis (Fig. 1c). A mirror operation in the D_{3h} symmetry and the lack of inversion symmetry in the monolayer play a crucial role to induce a novel valley Zeeman-type spin splitting in the band structure[22,23]. In the bilayer and the bulk case, two adjacent monolayers are rotated by π with respect to each other, which makes the whole structure centrosymmetric. Therefore their electronic states (bulk band structure shown in Fig. 1d) remain spin degenerate because of the inversion symmetry combined with time-reversal symmetry. As an effective way to induce inversion asymmetry in the bilayer or bulk WSe_2, applying a perpendicular external electric field can be used to regulate the band-spin splitting, as shown in WSe_2 band structures with and without perpendicular electric field E_{ex} (Supplementary Fig. 1a,b, respectively). Importantly, with inversion symmetry breaking, carriers in opposite valleys (with respect to the Γ point) in the Brillouin zone have opposite spin angular momenta because the system is time-reversal-symmetry protected. This indicates that valley-dependent phenomena should

[1]Geballe Laboratory for Advanced Materials, Stanford University, Stanford, California 94305, USA, [2]Stanford Institute for Materials and Energy Sciences, SLAC National Accelerator Laboratory, Menlo Park, California 94025, USA, [3]State Key Laboratory of Artificial Microstructure and Mesoscopic Physics, School of Physics, Peking University, Beijing 100871, China, [4]Collaborative Innovation Centre of Quantum Matter, Beijing 100871, China.
*e-mail: hyhwang@stanford.edu; yicui@stanford.edu

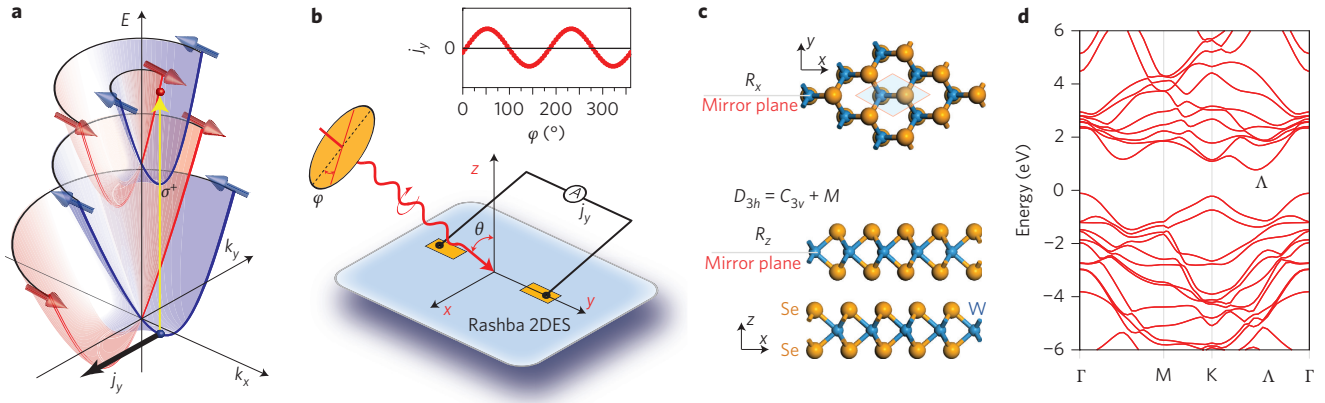

Figure 1 | Schematic diagrams of the CPGE based on Rashba spin splitting, and the crystal/electronic structure of layered 2H-WSe_2. a, A schematic band diagram for spin-orientation-induced CPGE for the direct optical transition in a 2DES with Rashba spin splitting. σ^+-excitation induces inter-subband transitions (yellow line; blue and red dots represent the generated hole and electron, respectively) in the conduction band, where the spin splitting together with the optical selection rules create the unbalanced occupation of the positive (k_y^+) and negative (k_y^-) states and further yield the spin-polarized photocurrent j_y. Blue and red arrows are spins with opposite directions. **b**, A schematic diagram for the CPGE measurement with a light incident angle θ to the normal direction. The helicity of laser light was modulated by a rotatable quarter-wave plate (yellow circle) with an angle of φ, following the relationship $P_{circ} = \sin 2\varphi$. As shown in the inset, the generated CPGE current j_y depend on the helicity of the radiation field: it reverses its direction on changing the radiation helicity from left handed to right handed. **c**, Top and side views of the layered structure of 2H-WSe_2. The D_{3h} symmetry ($C_{3v} + M$) of each Se–W–Se monolayer includes mirror operations (M), which play an important role for the generation of the CPGE current. **d**, Electronic band structure of bulk 2H-WSe_2, in which the conduction-band minimum sits at a non-symmetric point (defined as the Λ point) along the Γ–K direction. When electrons are doped into the WSe_2 system, Fermi pockets appear around the Λ points.

also be spin dependent, which implies the possibility of generating a spin-coupled valley current in WSe_2.

We fabricated WSe_2 single-crystal flakes into EDLTs, which have the capability to generate a large interfacial electric field to control electronic phases of solids[24–30] and modulate the spin texture in 2DESs[22,31,32]. Figure 2a is a cross-section diagram of a WSe_2 EDLT gated with ionic gel[33]. This large local interface electric field applied perpendicularly to the 2D plane can effectively modify interfacial band bending and the degree of inversion asymmetry at the WSe_2 surface. Such a surface band bending and resulting electron confinement within ~2 nm from the surface (the thickness of the accumulation layer depends on how large the external electric field is) plays an important role for the generation of the photocurrent carrying the spin–valley polarization information (discussed below). Owing to the band bending caused by the chemical potential alignment between the gel and the WSe_2, there is an electron accumulation of low carrier density at the gel/WSe_2 interface even before the external gate voltage V_G is applied.

Generation and electric-field control of the circular photogalvanic current. CPGE measurements induced by circularly polarized light on WSe_2 were used to detect a non-uniform distribution of photoexcited carriers and the generated spin-related photocurrent (j_y) in WSe_2, with the configuration shown in Fig. 2a. The photon energy (1.17 eV) used here is smaller than the indirect bandgap of WSe_2 (therefore the bandgap optical transition does not need to be considered in this study); thus, the photocurrent generated originates from the surface accumulation layer, and not from electron–hole excitations in bulk. To isolate the photocurrent response from a background current caused by laser-heating gradients in the sample, we swept the laser spot across two electrodes for different heat gradients in the zero-biased WSe_2 EDLT device (Fig. 2b) with a fixed incident angle ($\theta = 60°$) and a fixed polarization. The photocurrent switches its polarity as the laser spot is swept across the sample, but gives a non-zero finite value at the sample centre ($y = 0$), which would be a zero net current if the current originates only from the symmetric heating gradient. The observation of such a non-zero j_y value at $y = 0$ indicates that the generation of photocurrent might be caused by the non-uniform distribution of photoexcited carriers.

To confirm the dependence of the generated photocurrent on the helicity of the radiation light, the light-polarization dependence of j_y is measured at $y = 0$ with different incident angles θ (Fig. 2d–i and Supplementary Fig. 3). The first thing to be addressed here is the θ dependence of CPGE current j_{CPGE}, which shows that the peak behaviour (centred at around $\theta = 60°$ (Fig. 2c)) is quite similar to the CPGE current observed in Rashba 2DESs. Second, one can see that when light is obliquely incident with a non-zero θ, the obtained photocurrent j_y exhibits a strong dependence on light circular polarization and oscillates with the rotation angle φ of the quarter-wave plate. This j_y, which can be quantitatively expressed as $j_y = C\sin 2\varphi + L\sin 4\varphi + A$ (here A is other components of the Fourier series expansion), mainly includes two components, a π-periodic current oscillation term, $j_{CPGE} = C\sin 2\varphi$, corresponding to the CPGE current, and a π/2-period oscillation term $L\sin 4\varphi$, corresponding to the linear photogalvanic effect (discussed in Supplementary Section 8). The existence of a $j_{CPGE} = C\sin 2\varphi$ component (red curves) that satisfies the amplitude expression $j_{CPGE} = \eta\gamma I \sin\theta \sin 2\varphi$ directly reflects the helicity of the generated photocurrent. As indicated in Fig. 2d–i, the direction and magnitude of this j_{CPGE} strongly depend on the degree of circular polarization of the incident light, and j_{CPGE} reverses its direction on changing the radiation helicity from left handed to right handed[8,31].

The CPGE phenomenon and the spin photocurrent in Rashba 2DESs are highly sensitive to subtle details of the electronic band structure, and even a small band splitting may result in measurable effects. Therefore, the modification of the degree of inversion asymmetry with an external perpendicular electric field can provide us with a simple way to control the CPGE photocurrent in the WSe_2 system. Figure 3 and Supplementary Fig. 5 show the light-polarization dependent j_y, obtained in a WSe_2 EDLT at external bias V_G varied from zero to 1.1 V. As a common point, the magnitude of the electric current j_y for all bias is related to the radiation helicity, and j_{CPGE} (red curves) follows $C\sin 2\varphi$. Importantly, j_{CPGE} dramatically increases with V_G from tens of picoamps to thousands of picoamps

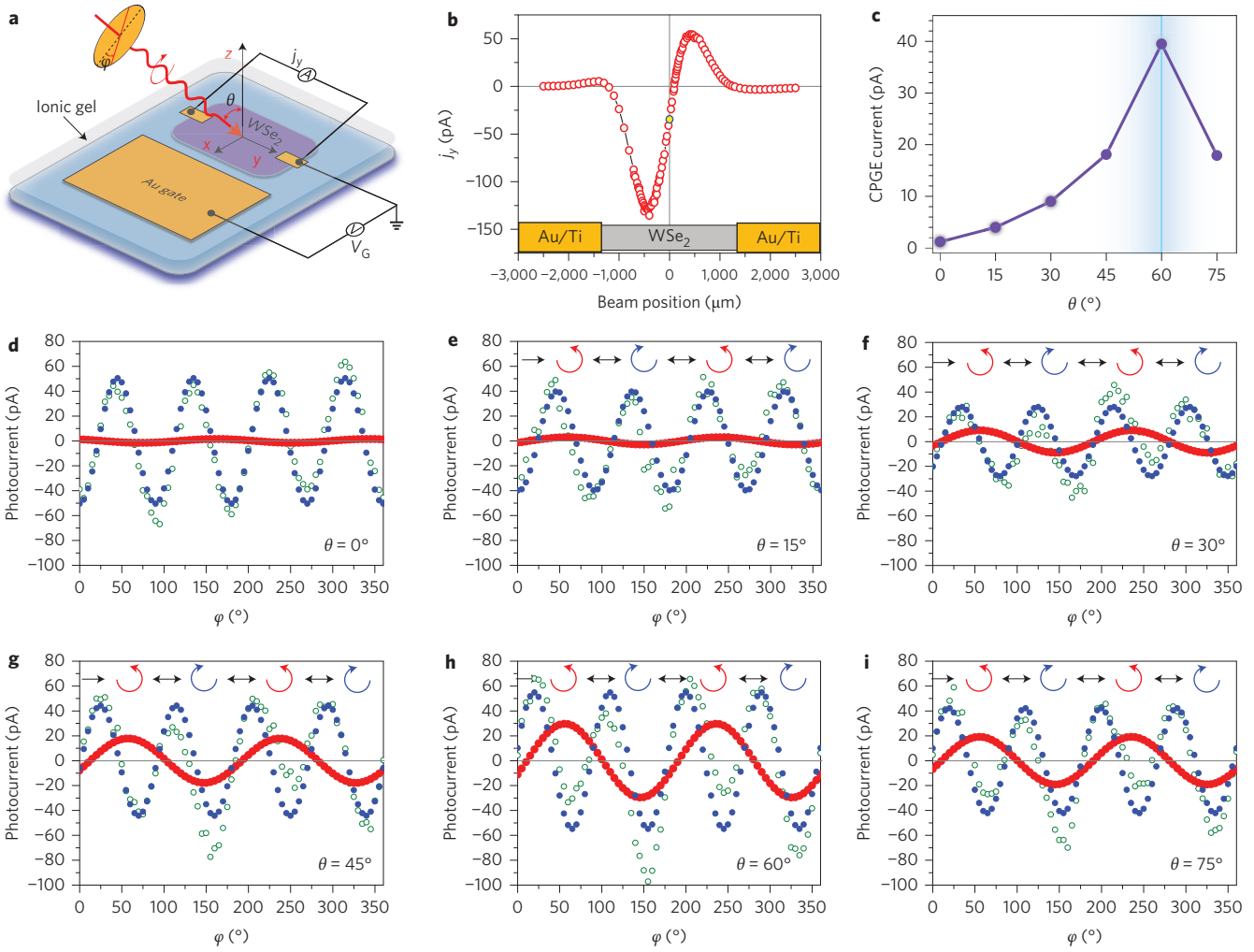

Figure 2 | Schematic diagram and incident angle-dependent CPGE measurement of ambipolar WSe_2 EDLTs. a, Schematic structure of a typical WSe_2 EDLT with ionic gel gating. By applying a gate voltage V_G to the lateral Au gate electrode, ions in the gel are driven to the WSe_2 surface, forming a perpendicular electric field at the EDL interface. Even without an external bias, a relatively low carrier-density accumulation layer exists at the WSe_2 surface owing to the Fermi level realignment between the gel/WSe_2 interface. **b**, A position-dependent photocurrent from sweeping the laser spot across the two electrodes (yellow rectangles shown at the bottom) in the zero-biased WSe_2 EDLT device with a fixed polarization. **c**, CPGE photocurrent j_{CPGE} as a function of the incident angle, θ, which shows a peak around $\theta = 60°$ (indicated by the blue line). **d–i**, Light polarization dependence of photocurrent j_y in a biased WSe_2 EDLT, measured at $y = 0$ with different incident angles θ. The open green circles are the measured j_y following the form $j_y = C\sin2\varphi + L\sin4\varphi + A$. The filled blue circles are the photocurrent that originates from the linear photogalvanic effect and obtained from the $\pi/2$-period oscillation term $L\sin4\varphi$ by fitting. The filled red dots are the CPGE photocurrent with a π-periodic current oscillation. Polarization of the incident light at each quarter-wave plate angle, φ, is given by the symbols shown in the inset of each figure.

(Supplementary Fig. 3m,n), which unambiguously indicates an electric modulation of the CPGE photocurrent. Such an electric modulation was very reproducible and observed in multiple devices.

To understand how photons transfer their angular momentum to electrons and further induce the photocurrent, we compared the magnitude of the photocurrent at $V_G = 0.3$ V under three special incidence angles, as shown in Fig. 4a,c,e. In most cases shown in Fig. 2a, where the photocurrent is generated transverse to the light scattering plane (x–z plane), the opposing angular-momentum polarizations that are excited by the different helicities must have an angular-momentum component in the x–z plane and be asymmetrically distributed along the y direction in k-space. When light is obliquely incident in the y–z plane, where the azimuth angle $\phi = 90°$ (the angle between the x axis and the projection of incident light in the x–y plane, shown in Fig. 4c), one can see that the photocurrent completely disappears (Fig. 4d) because the device's metal contacts lie in the light-scattering plane while the current flows in the direction perpendicular to this plane. This indicates that the electrons involved in generating the photocurrent have an angular momentum polarization that is locked perpendicular to their momentum. In the particular scenario with normally incident light (Fig. 4e,f), the photocurrent is negligibly small because it is forbidden by the rotation symmetry (C_{3v}) about the normal axis. By considering these observations, the results reveal that the important features of the helicity-dependent photocurrent j_{CPGE} arise from the asymmetric optical excitation of the splitting bands. The magnitude and direction of CPGE photocurrent strongly depend on the helicity of the incident circularly polarized light, clearly giving us proof that the generated current has a direct relationship with the modulation of angular momentum (either spin or orbital angular momentum) near WSe_2 valleys, even though we cannot experimentally distinguish which angular momentum is modulated by the circularly polarized light, either the spin or orbital angular momentum (or both). The theoretical analysis of the orbital component and the

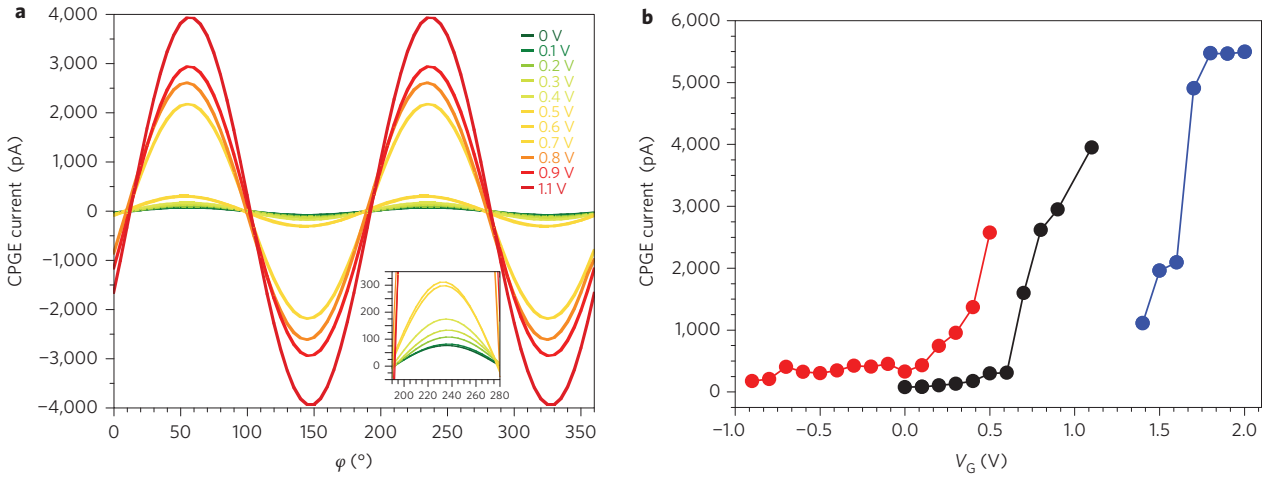

Figure 3 | Electric field modulation of the spin photocurrent in WSe_2 EDLTs. a, The electric field modulation of the CPGE current j_{CPGE} in WSe_2 EDLTs at various gate voltages V_G. Inset: Expanded picture of the CPGE current j_{CPGE} at low V_G. **b**, CPGE current j_{CPGE} as a function of V_G. The magnitude of the j_{CPGE} can be modulated to a level above two orders larger than that of the zero bias case, which provides a new way to a direct modulation of the spin photocurrent. The black, red and blue filled circles are from different samples.

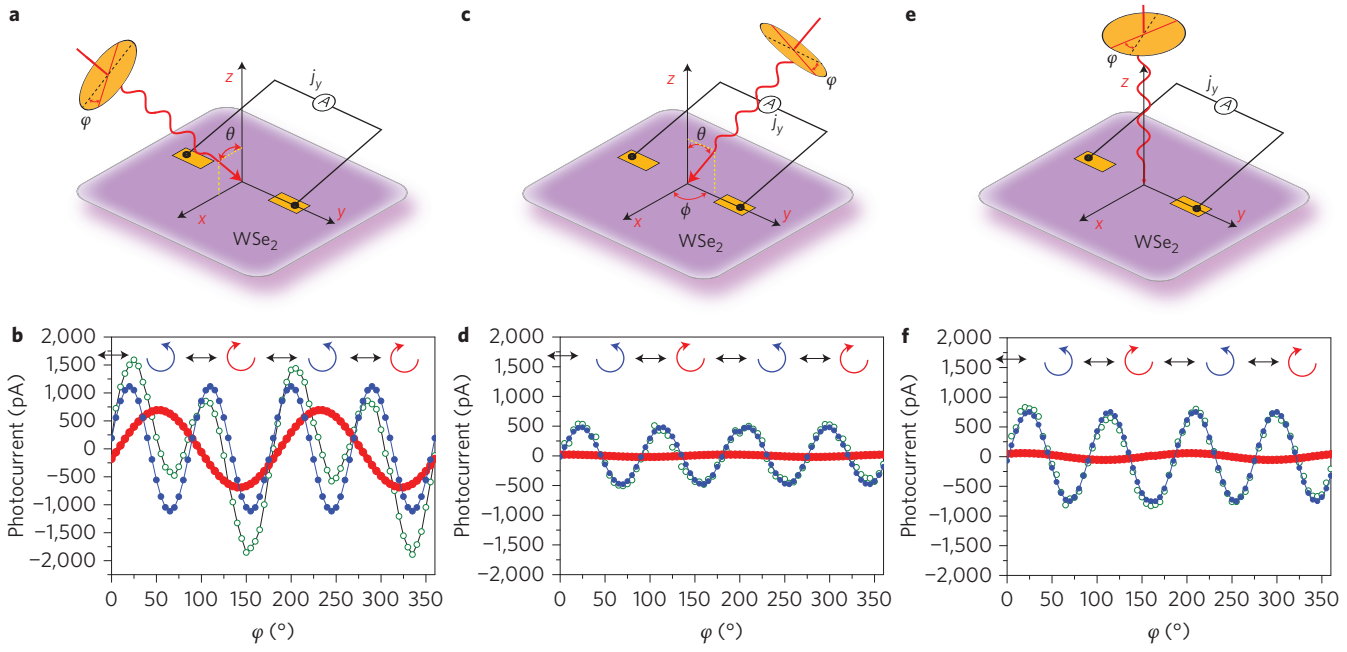

Figure 4 | Light-polarization-dependent photocurrent in biased WSe_2 EDLTs with different incidence angles. a,**b**, Configuration (**a**) and CPGE measurement (**b**) with the photocurrent generated transverse to the light scattering plane (*x*-*z* plane). Polarization of the incident light at each quarter-wave plate angle, φ, is given by the symbols shown in the inset of **b**. **c**–**f**, Configuration (**c**) and CPGE measurement (**d**) with light obliquely incident (at angle θ =60°) in the *y*-*z* plane, and with normally incident light (**e** and **f**, respectively). All measurements in this figure were performed at V_G = 0.3 V.

spin texture (in Supplementary Section 1) can clearly give us the corresponding information on how the spin and valley indices are involved with the photocurrent.

Absence of the CPGE photocurrent without inversion symmetry breaking. We now show theoretically how the CPGE phenomenon is related to valley polarization in the WSe_2 band structure. As the Fermi energy can be tuned into the lowest conduction band with gel gating, the Fermi surface is located at six valleys around the *z* direction momentum $k_z = 0$ plane, as shown in Fig. 5a. The centre of each valley (denoted as Λ_i or Λ_i' for convenience) lies in the ΓK_i or $\Gamma K_i'$ direction (Fig. 5b) and all the optical transitions will be direct transitions within the conduction band near these Λ_i valleys. With broken inversion symmetry, different valleys can be distinguished by the Berry phase of the Bloch bands[14], which gives rise to the valley-dependent optical selection rule in WSe_2.

The photocurrent j_{CPGE} can be derived by considering the light absorption of electrons that occur at six valley points Λ_i and Λ_i' in the lower conduction bands. We first consider the electron-transition amplitude caused by photon absorption at valley point Λ_2. The electron–photon interaction takes the form:

$$H' = \int d\mathbf{r}^3 (ie\hbar/mc)\mathbf{A}(\mathbf{r}) \cdot \nabla$$

where $\mathbf{A}(\mathbf{r})$ is the vector potential of the photons, e and m are the electron's charge and mass, and c is the speed of light. To the

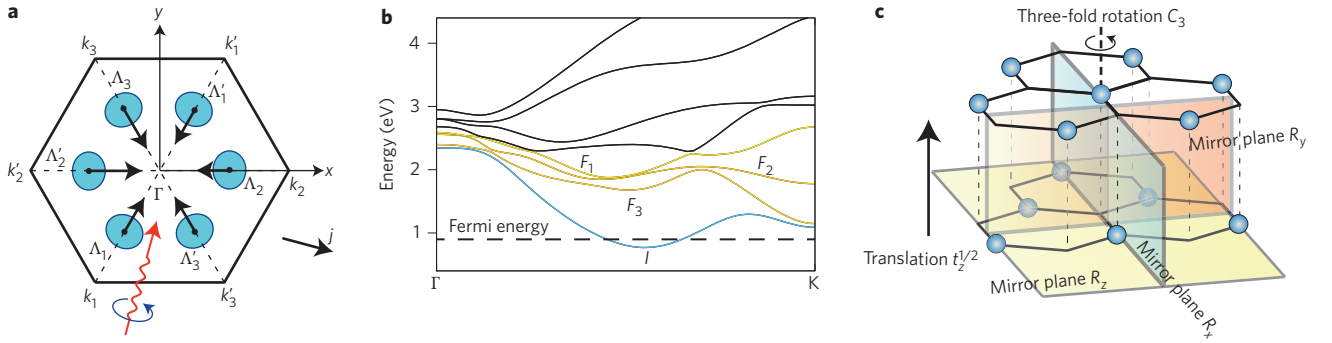

Figure 5 | Physical origin of the generation of spin-coupled valley photocurrent in WSe_2 EDLTs and its electric field modulation. a, The interpretation of the CPGE in reciprocal space. The hexagon represents the Brillouin zone of WSe_2 in the $k_z = 0$ plane. The Fermi surface consists of six electron pockets (in blue) at Λ_i. When circularly polarized light (red arrow) with a specific helicity (blue circular arrow) is applied, a photocurrent (black arrow) is induced at each pocket Λ_i, yielding a net current j perpendicular to the incident light. **b**, Electronic band structure (conduction band) of 3D bulk WSe_2. CPGE arises when the Fermi energy is tuned into band I. The electrons are excited into higher bands F_1, F_2 and F_3. **c**, Illustration of the crystal symmetries of WSe_2. For simplicity, only W atoms are plotted. The crystal has rotation symmetry C_{3v}, mirror reflection symmetries R_x and R_z with respect to the planes shown in the figure and a non-symmorphic symmetry $Y = t_z^{1/2} \otimes R_y$ that interchanges the two layers.

leading order, the momentum of the incident photon can be neglected compared to the electron momentum, and $\mathbf{A}(\mathbf{r}) = \mathbf{A}$ is therefore a constant vector. We denote the initial state with momentum $\mathbf{k}_{\Lambda_2}$ in the lowest conduction band as $|I, \mathbf{k}_{\Lambda_2}\rangle$, and the final state in the higher conduction band as $|F, \mathbf{k}_{\Lambda_2}\rangle$. They have energies ϵ_I and ϵ_F, respectively. The transition amplitude is then of the form:

$$\mathcal{M}_2(\mathbf{A}) = \mathcal{M}_{2,x}A_x + \mathcal{M}_{2,y}A_y + \mathcal{M}_{2,z}A_z = \boldsymbol{\mathcal{M}}_2 \cdot \mathbf{A}$$

where $\mathcal{M}_{2,u} = (e\hbar/mc)\langle F, \mathbf{k}_{\Lambda_2}|i\partial_u|I, \mathbf{k}_{\Lambda_2}\rangle$ for $u = x$, y and z. The transition from band I to F varies the electron's group velocity from $\nabla_{\mathbf{k}}\epsilon_I$ to $\nabla_{\mathbf{k}}\epsilon_F$, which are dominantly along the direction of $\mathbf{k}_{\Lambda_2}$, so the current produced at Λ_2 is:

$$\mathbf{j}_{\Lambda_2} = \frac{\xi I}{A^2}\mathbf{e}_2\left|\boldsymbol{\mathcal{M}}_2 \cdot \mathbf{A}(\theta, \phi)\right|^2$$

where $\mathbf{e}_i = \mathbf{k}_{\Lambda_i}/|\mathbf{k}_{\Lambda_i}|$ is the unit vector along the ΓK_i direction, θ and ϕ are the incident and azimuth angles, respectively, of the light, I is the incident light intensity, $A = |\mathbf{A}|$ and ξ is a coefficient proportional to the velocity difference $|\nabla_{\mathbf{k}}\epsilon_F - \nabla_{\mathbf{k}}\epsilon_I|$ and positively correlated to the carrier density. The currents produced at other valleys Λ_i can be obtained through a C_3 rotation. The amplitude at valley Λ'_i is related to that at Λ_i through the time-reversal symmetry T, $\boldsymbol{\mathcal{M}}'_2 = -\boldsymbol{\mathcal{M}}_2^*$. The total current can be expressed as:

$$\mathbf{j} = \frac{\xi I}{A^2}\sum_{i=1}^{3}\mathbf{e}_i\left(\left|\boldsymbol{\mathcal{M}}_2 \cdot \mathbf{A}\left(\theta, \phi - \frac{2(i-2)\pi}{3}\right)\right|^2 - \left|\boldsymbol{\mathcal{M}}_2^* \cdot \mathbf{A}\left(\theta, \phi - \frac{2(i-2)\pi}{3}\right)\right|^2\right)$$

where we assume six valleys have the same carrier densities (Supplementary Section 5). The condition for a non-zero $\boldsymbol{j}$ is $\boldsymbol{\mathcal{M}}_2^* \neq c_{\mathrm{ph}}\boldsymbol{\mathcal{M}}_2$, where c_{ph} is a phase factor (see Supplementary Section 4). Our task, then, is to find $\boldsymbol{\mathcal{M}}_2$.

The spin–orbit coupling (SOC), though strong in WSe_2, is not essential to generate the CPGE in a material with C_{3V} symmetry. To show this, we set the SOC to zero for the moment, and see how the photocurrent arises simply based on valley-dependent optical selection rules. The electron states near the Fermi surface are mainly composed of d orbitals (Supplementary Fig. 2). In the absence of the perpendicular external electric field, the crystal has time-reversal symmetry T, mirror reflection symmetries R_x ($x \to -x$) and R_z ($z \to -z$), and a non-symmorphic symmetry $Y = t_z^{1/2} \otimes R_y (y \to -y)$ that interchanges the two monolayers in a unit cell, where t_z is the unit translation along the z direction (Fig. 5c). This indicates the electron states at Λ_2 are eigenstates of the symmetries R_z, Y and TR_x. In particular, $Y^2 = t_z = 1$ for $k_z = 0$, and therefore $Y = \pm 1$. Combining with *ab initio* calculations (see Supplementary Fig. 2), we find the initial state of the form $|I, \mathbf{k}_{\Lambda_2}\rangle = ia_0|d^+_{xy}\rangle + b_0|d^+_{x^2-y^2}\rangle + c_0|d^+_{3z^2-r^2}\rangle$, where $|d^\pm_{f(x,y,z)}\rangle$ denotes the Bloch state

$$(1/\sqrt{V})\sum_j e^{i\mathbf{k}_{\Lambda_2}\cdot\mathbf{r}_j}|d^\pm_{j,f(x,y,z)}\rangle$$

with $Y = \pm 1$. Within reach of the photon energy, there are three states in the higher conduction bands (Fig. 5b):

$$|F_1, \mathbf{k}_{\Lambda_2}\rangle = ia_1|d^+_{xy}\rangle + b_1|d^+_{x^2-y^2}\rangle + c_1|d^+_{3z^2-r^2}\rangle$$

$$|F_2, \mathbf{k}_{\Lambda_2}\rangle = |d^+_{yz}\rangle$$

$$|F_3, \mathbf{k}_{\Lambda_2}\rangle = ia_3|d^-_{xy}\rangle + b_3|d^-_{x^2-y^2}\rangle + c_3|d^-_{3z^2-r^2}\rangle$$

All the coefficients a_i, b_i and c_i are real, as is required by TR_x symmetry. Owing to the R_z and Y symmetries, the only non-vanishing amplitude from $|I, \mathbf{k}_{\Lambda_2}\rangle$ to $|F_1, \mathbf{k}_{\Lambda_2}\rangle$ is the x component $\mathcal{M}_{2,x}^{(I\to F_1)}$. This means $\boldsymbol{\mathcal{M}}_2^{(I\to F_1)} = \mathcal{M}_{2,x}^{(I\to F_1)}\mathbf{e}_x = c_{\mathrm{ph}}\boldsymbol{\mathcal{M}}_2^{(I\to F_1)^*}$, and the transition from band I to F_1 gives a net current zero. Similarly, the only non-vanishing amplitudes from $|I, \mathbf{k}_{\Lambda_2}\rangle$ to $|F_2, \mathbf{k}_{\Lambda_2}\rangle$ and to $|F_3, \mathbf{k}_{\Lambda_2}\rangle$ are $\mathcal{M}_{2,z}^{(I\to F_2)}$ and $\mathcal{M}_{2,y}^{(I\to F_3)}$, respectively, and they also produce no net current (see Supplementary Section 4 for details). So the net photocurrent is zero in the absence of the external out-of-plane electric field E_{ex}, which breaks inversion symmetry. Though we deduce this conclusion from a 3D analysis, it is also true for 2D ultrathin films that do not have a Y symmetry (see Supplementary Sections 6 and 7 for details).

Spin-coupled valley photocurrent generated under external electric fields. Next we discuss how E_{ex} generates the photocurrent and modulates its magnitude. When an perpendicular electric field $\mathbf{E}_{\mathrm{ex}} = E_{\mathrm{ex}}\mathbf{e}_z$ is applied, the WSe_2 crystal loses the mirror reflection symmetry R_z. As the two states $|F_1, \mathbf{k}_{\Lambda_2}\rangle$ and $|F_2, \mathbf{k}_{\Lambda_2}\rangle$ have opposite R_z eigenvalues and are close

in energy, this symmetry breaking induces a mix between the two states. For weak field E_{ex}, the two new eigenstates take the form $|F_1', \mathbf{k}_{\Lambda_2}\rangle = |F_1, \mathbf{k}_{\Lambda_2}\rangle + gE_{ex}|F_2, \mathbf{k}_{\Lambda_2}\rangle$ and $|F_2', \mathbf{k}_{\Lambda_2}\rangle = |F_2, \mathbf{k}_{\Lambda_2}\rangle - gE_{ex}|F_1, \mathbf{k}_{\Lambda_2}\rangle$, where g is real as required by the TR_x symmetry. In the above we have found the transition amplitude to $|F_1, \mathbf{k}_{\Lambda_2}\rangle$ and $|F_2, \mathbf{k}_{\Lambda_2}\rangle$, so it is straightforward to show that the transition amplitude to $|F_1', \mathbf{k}_{\Lambda_2}\rangle$ has two non-vanishing components $\mathcal{M}_{2,x}^{(I\to F_1')}$ and $\mathcal{M}_{2,z}^{(I\to F_1')} = m_{2,z}^{(I\to F_1')}E_{ex}$ (see Supplementary Section 7). Owing to the TR_x symmetry, $\mathcal{M}_{2,x}^{(I\to F_1')}$ is real and $\mathcal{M}_{2,z}^{(I\to F_1')}$ is purely imaginary. Therefore $\boldsymbol{\mathcal{M}}_2^{(I\to F_1')^*} \neq c_{ph}\boldsymbol{\mathcal{M}}_2^{(I\to F_1')}$, which satisfies the condition to obtain a non-zero $\boldsymbol{j}$ in WSe_2, as we have observed in the experiments. The same analysis applies to the transition amplitude $\boldsymbol{\mathcal{M}}_2^{(I\to F_2')}$ to $|F_2', \mathbf{k}_{\Lambda_2}\rangle$. These constitute the two channels that induce the CPGE. For circular polarized light obtained via a rotation angle φ quarter-wave plate with incident angle θ and azimuth angle ϕ, the vector potential is:

$$\boldsymbol{A}(\theta, \phi) = A\Big[(\mathbf{e}_x \sin\phi - \mathbf{e}_y \cos\phi)(1 + i\cos 2\varphi) + i(\mathbf{e}_z \sin\theta - \mathbf{e}_x \cos\theta\cos\phi - \mathbf{e}_y \cos\theta \sin\phi)\sin 2\varphi\Big]$$

A direct calculation shows the net current $\mathbf{j}$ is given by:

$$\mathbf{j} = \chi I E_{ex} \sin\theta \sin 2\varphi \mathbf{e}_\perp$$

where $\mathbf{e}_\perp = (\mathbf{e}_x \sin\phi - \mathbf{e}_y \cos\phi)$ is the in-plane unit vector perpendicular to the incident light, and the coefficient $\chi = 12g(\xi_1' - \xi_2')\left|\mathcal{M}_{2,x}^{(I\to F_1)}\mathcal{M}_{2,z}^{(I\to F_2)}\right|$ (see Supplementary Section 7). As the coefficient ξ_i' is related to the electron filling controlled by the gating voltage, the coefficient $\chi = \chi(E_{ex})$ is also implicitly an increasing function of E_{ex}. Considering that there is another E_{ex} term in the equation for $\mathbf{j}$, the photocurrent can therefore be prominently tuned through the gating electric field E_{ex} in a nonlinear way (proportional to $\chi(E_{ex})E_{ex}$; more details are given in Supplementary Section 7). For $gE_{ex} \approx 10^{-2}$, an order of magnitude estimation gives a photocurrent in the range 10^{-10} A to 10^{-9} A (Supplementary Section 7), in agreement with the experimental observations shown in Figs 2–4.

The current, which is perpendicular to the incident direction of the light, should be defined as a pure valley-polarized current without the need to consider the SOC[9,10,34,35]. Once SOC is introduced, the spin degeneracy is removed, and the transition amplitude of electrons with opposite spins becomes different. The photocurrent $\boldsymbol{j}$ then becomes a partially spin-polarized photocurrent based on the valley polarized current (discussed in detail in Supplementary Section 7), which gives us the intrinsic nature of the observed spin-coupled valley photocurrent. As SOC is not a prominent effect here, the spin current could be one or two orders smaller than the total photocurrent.

We demonstrate here the generation of the spin and valley polarized photocurrent in a WSe_2 EDLT and the control of this current with both the helicity of circularly polarized light and the magnitude of the broken inversion symmetry at a WSe_2 surface by the perpendicular electric field. Such generation and electric control of the spin-coupled valley photocurrent in a transistor configuration exhibit great potential towards the realization of practical applications, as well as the physics for manipulating the spin and valley degrees of freedom in WSe_2. Given that this mechanism for achieving and modulating the spin photocurrent should not be limited to these MX_2 dichalcogenides (such as MoS_2, $MoSe_2$ or WS_2), our finding can be generalized to other 2DESs with valleys near the corners of a hexagonal Brillouin zone, and thereby pave a new path towards developing spintronics/valleytronic devices.

Methods

Two Ti/Au electrodes were fabricated on a freshly cleaved WSe_2 single-crystal flake (on a SiO_2/Si wafer) with a channel a few millimetres in length. Serving as the side-gate electrode, a large-area Au pad was deposited near the WSe_2, but electrically insulated from the WSe_2. A typical EDLT was fabricated by drop-casting a DEME-TFSI-based ionic gel (DEME-TFSI, *N*,*N*-diethyl-*N*-(2-methoxyethyl)-*N*-methylammonium bis(trifluoromethylsulfonyl)imide, from the Kanto Chemical Co). WSe_2 transistors can be obtained based on gel gating. The flake thickness is irrelevant to the experimental observations because all the phenomena occur at the surface accumulation layer of WSe_2 (where the surface inversion symmetry occurs) and do not involve the bulk information. The CPGE measurement configurations are shown in Fig. 2a and Supplementary Fig. 3. The solid-state laser with a wavelength 1,064 nm (1.17 eV, smaller that the indirect bandgap of WSe_2) was intentionally chosen in this study to avoid the excitation from the valence band to the conduction band. To produce photocurrent, the laser beam with a 500 μm diameter spot is incident on the device at the centre between the two electrodes with the out-of-plane angle θ (defined as the angle of incident light from the normal of the x–y plane). The helicity of laser light was modulated by a rotatable quarter-wave plate, $P_{circ} = \sin 2\varphi$. The polarization-dependent photocurrent was identified by measuring j_y collected between two electrodes by an a.c. lock-in amplifier. All the measurements on the spin photocurrent generation were performed at room temperature.

Electronic structure calculations were carried out by the Vienna Ab-initio Simulation Package (VASP)[36,37] within the framework of the Perdew–Burke–Ernzerhof-type generalized gradient approximation[38] of density functional theory[39]. SOCs are fully considered. The kinetic energy cutoff is set to 450 eV in all calculations. A $12 \times 12 \times 6$ grid is used for the k-mesh of the bulk calculation. The lattice constant and internal atomic positions are taken from experiments[40]. The external electric field was modelled by adding a dipole potential along the surface normal, that is the (001) direction.

Received 22 February 2014; accepted 30 July 2014; published online 7 September 2014

References

1. Murakami, S., Nagaosa, N. & Zhang, S. C. Dissipationless quantum spin current at room temperature. *Science* **301,** 1348–1351 (2003).
2. Awschalom, D. D. & Flatte, M. E. Challenges for semiconductor spintronics. *Nature Phys.* **3,** 153–159 (2007).
3. Zutic, I., Fabian, J. & Das Sarma, S. Spintronics: fundamentals and applications. *Rev. Mod. Phys.* **76,** 323–410 (2004).
4. Ganichev, S. D. *et al.* Spin-galvanic effect. *Nature* **417,** 153–156 (2002).
5. Kikkawa, J. M. & Awschalom, D. D. Lateral drag of spin coherence in gallium arsenide. *Nature* **397,** 139–141 (1999).
6. Ivchenko, E. L. & Ganichev, S. D. in *Spin Physics in Semiconductors* (ed. Dyakonov, M. I.) 245–277 (Springer Series in Solid Sciences 157, Springer, 2008).
7. Ganichev, S. D. & Prettl, W. Spin photocurrents in quantum wells. *J. Phys. Condens. Matter* **15,** R935–R983 (2003).
8. McIver, J. W., Hsieh, D., Steinberg, H., Jarillo-Herrero, P. & Gedik, N. Control over topological insulator photocurrents with light polarization. *Nature Nanotech.* **7,** 96–100 (2012).
9. Karch, J. *et al.* Photoexcitation of valley-orbit currents in (111)-oriented silicon metal–oxide-semiconductor field-effect transistors. *Phys. Rev. B* **83,** 121312 (2011).
10. Karch, J. *et al.* Orbital photogalvanic effects in quantum-confined structures. *J. Phys. Condens. Matter* **22,** 355307 (2010).
11. Bychkov, Y. A. & Rashba, E. I. Properties of a 2*d* electron-gas with lifted spectral degeneracy. *J. Exp. Theor. Phys. Lett.* **39,** 78–81 (1984).
12. Winkler, R. Spin orientation and spin precession in inversion-asymmetric quasi-two-dimensional electron systems. *Phys. Rev. B* **69,** 045317 (2004).
13. Xiao, D., Liu, G. B., Feng, W. X., Xu, X. D. & Yao, W. Coupled spin and valley physics in monolayers of MoS_2 and other group-VI dichalcogenides. *Phys. Rev. Lett.* **108,** 196802 (2012).
14. Yao, W., Xiao, D. & Niu, Q. Valley-dependent optoelectronics from inversion symmetry breaking. *Phys. Rev. B* **77,** 235406 (2008).
15. Rycerz, A., Tworzydlo, J. & Beenakker, C. W. J. Valley filter and valley valve in graphene. *Nature Phys.* **3,** 172–175 (2007).
16. Xiao, D., Yao, W. & Niu, Q. Valley-contrasting physics in graphene: magnetic moment and topological transport. *Phys. Rev. Lett.* **99,** 236809 (2007).
17. Mak, K. F., He, K. L., Shan, J. & Heinz, T. F. Control of valley polarization in monolayer MoS_2 by optical helicity. *Nature Nanotech.* **7,** 494–498 (2012).
18. Zeng, H. L., Dai, J. F., Yao, W., Xiao, D. & Cui, X. D. Valley polarization in MoS_2 monolayers by optical pumping. *Nature Nanotech.* **7,** 490–493 (2012).
19. Cao, T. *et al.* Valley-selective circular dichroism of monolayer molybdenum disulphide. *Nature Commun.* **3,** 887 (2012).
20. Jones, A. M. *et al.* Optical generation of excitonic valley coherence in monolayer WSe_2. *Nature Nanotech.* **8,** 634–638 (2013).

21. Ross, J. S. *et al.* Electrical control of neutral and charged excitons in a monolayer semiconductor. *Nature Commun.* **4,** 1474 (2013).
22. Yuan, H. T. *et al.* Zeeman-type spin splitting controlled by an electric field. *Nature Phys.* **9,** 563–569 (2013).
23. Zhu, Z. Y., Cheng, Y. C. & Schwingenschlogl, U. Giant spin-orbit-induced spin splitting in two-dimensional transition-metal dichalcogenide semiconductors. *Phys. Rev. B* **84,** 153402 (2011).
24. Yuan, H. T. *et al.* High-density carrier accumulation in ZnO field-effect transistors gated by electric double layers of ionic liquids. *Adv. Funct. Mater.* **19,** 1046–1053 (2009).
25. Efetov, D. K. & Kim, P. Controlling electron–phonon interactions in graphene at ultrahigh carrier densities. *Phys. Rev. Lett.* **105,** 256805 (2010).
26. Dhoot, A. S., Israel, C., Moya, X., Mathur, N. D. & Friend, R. H. Large electric field effect in electrolyte-gated manganites. *Phys. Rev. Lett.* **102,** 136402 (2009).
27. Ueno, K. *et al.* Discovery of superconductivity in $KTaO_3$ by electrostatic carrier doping. *Nature Nanotech.* **6,** 408–412 (2011).
28. Bollinger, A. T. *et al.* Superconductor–insulator transition in $La_{2-x}Sr_xCuO_4$ at the pair quantum resistance. *Nature* **472,** 458–460 (2011).
29. Yamada, Y. *et al.* Electrically induced ferromagnetism at room temperature in cobalt-doped titanium dioxide. *Science* **332,** 1065–1067 (2011).
30. Jeong, J. *et al.* Suppression of metal–insulator transition in VO_2 by electric field-induced oxygen vacancy formation. *Science* **339,** 1402–1405 (2013).
31. Yin, C. M. *et al.* Tunable surface electron spin splitting with electric double-layer transistors based on InN. *Nano Lett.* **13,** 2024–2029 (2013).
32. Shibata, K., Yuan, H. T., Iwasa, Y. & Hirakawa, K. Large modulation of zero-dimensional electronic states in quantum dots by electric-double-layer gating. *Nature Commun.* **4,** 2664 (2013).
33. Cho, J. H. *et al.* Printable ion-gel gate dielectrics for low-voltage polymer thin-film transistors on plastic. *Nature Mater.* **7,** 900–906 (2008).
34. Olbrich, P. *et al.* Observation of the orbital circular photogalvanic effect. *Phys. Rev. B* **79,** 121302 (2009).
35. Ezawa, M. Spin-valley optical selection rule and strong circular dichroism in silicene. *Phys. Rev. B* **86,** 161407 (2012).
36. Kresse, G. & Hafner, J. *Ab initio* molecular-dynamics for liquid-metals. *Phys. Rev. B* **47,** 558–561 (1993).
37. Kresse, G. & Joubert, D. From ultrasoft pseudopotentials to the projector augmented-wave method. *Phys. Rev. B* **59,** 1758–1775 (1999).
38. Perdew, J. P., Burke, K. & Ernzerhof, M. Generalized gradient approximation made simple. *Phys. Rev. Lett.* **77,** 3865–3868 (1996).
39. Hohenberg, P. & Kohn, W. Inhomogeneous electron gas. *Phys. Rev. B* **136,** 864–871 (1964).
40. Schutte, W. J., Deboer, J. L. & Jellinek, F. Crystal-structures of tungsten disulfide and diselenide. *J. Solid State Chem.* **70,** 207–209 (1987).

Acknowledgements

This work was supported by the Department of Energy, Office of Basic Energy Sciences, Division of Materials Sciences and Engineering, under contract DE-AC02-76SF00515. B.L., H-J.Z., G.X., H.Y.H. and S-C.Z. also acknowledge FAME, one of six centres of STARnet, a Semiconductor Research Corporation program sponsored by MARCO and DARPA. X-Q.W. and B.S. acknowledge the National Basic Research Program of China (No. 2012CB619300 and 2013CB921900) and the NSFC of China (No. 61225019, 11023003 and 61376060).

Author contributions

H-T.Y., X-Q.W. and B.L. contributed equally to this work. H-T.Y., H.Y.H. and Y.C. conceived and designed the experiments. H-T.Y. performed the sample fabrication and all optical and transport measurements. H-T.Y., X-F.F., X-Q.W. and B.S. performed the CPGE measurements. B.L., H-J.Z., G.X., Y.X. and S-C.Z. performed all the DFT calculations and theoretical analyses. S-C.Z., H.Y.H. and Y.C. supervised the project. H-T.Y., B.L. and H-J.Z. wrote the manuscript, with input from all authors.

Additional information

Supplementary information is available in the online version of the paper. Reprints and permissions information is available online at www.nature.com/reprints. Correspondence and requests for materials should be addressed to H.Y.H. and Y.C.

Competing financial interests

The authors declare no competing financial interests.